Spring 5-1-2022

Study of Porosity of Gelatin-Alginate Hydrogels to Model Brain Matter for Studying Traumatic Brain Injuries

Apolline Vincent
apolline.vincent@uconn.edu

Study of Porosity of Gelatin-Alginate Hydrogels to Model Brain Matter for Studying Traumatic Brain Injuries

An Honors Thesis Submitted to

the Department of Biomedical Engineering, University of Connecticut,

in Partial Fulfillment of the Requirements

for the Bachelor of Science Degree in Biomedical Engineering with Honors

Apolline Vincent

May 2022

Thesis Supervisor: Dr. Fayekah Assanah

Honors Advisor: Dr. Patrick Kumavor

Table of Contents

Table of Figures

Table of Tables

Abstract

Traumatic brain injuries (TBIs) affect brain tissue and neuronal signaling, leading to many side effects including death. Research on TBIs is limited by the lack of accurate brain matter models to study the physiological and cellular reaction. Alginate-gelatin hydrogels have been designed and modified to mimic the mechanical properties of the brain to act as an accurate *in vitro* model. This Honors thesis aims to verify the porous microstructure of gelatin-alginate hydrogels through Scanning Electron Microscopy (SEM) to understand how gelatin and alginate affect the microstructure. I measured the pore sizes of each hydrogel using *ImageJ*, compared the average pore size between concentrations, and determined the effect gelatin and alginate have on the diameter. The results of this thesis can be utilized by future researchers to better understand alginate/gelatin hydrogels, and the effects of alginate and gelatin concentration on the ability to encapsulate cells. This can pave the way for cell implantation in the hydrogels to study the cellular response of the brain when subjected to forces comparable to those caused by traumatic brain injuries.

1. Introduction

1.01 Motivation

Each year, there are around 50 million cases of traumatic brain injuries (TBIs) that are reported around the world from all age groups [1]. In 2019, the United States alone reported 61,000 deaths resulting from TBIs mostly related to firearm-related suicide but also due to falls, assault, motor vehicle accidents, sports-related injuries, and military injuries [2,3]. The statistics surrounding the prevalence and effects of TBIs display a major clinical problem and a gap in understanding of TBIs especially between the engineering and healthcare fields. This gap in understanding is mostly related to the limited research in understanding the cellular responses to the blunt forces during TBI.

Current research has observed that during TBIs, the brain makes direct contact with the intracranial surface of the skull which initiates an immune response at the site of impact. As a result, the body upregulates proinflammatory cytokines, promoting inflammation at the injury site and causing various negative pathological responses such as gliosis, demyelination of nerve fibers, and cell apoptosis [4]. The physical abrupt movement of the brain further leads to the stretching and tearing of axons within white matter tracts, which can ultimately cause necrotic apoptosis and disturbed neural vasculature [4].

1.02 Current Research – *In Vivo* Testing

Scientists and researchers have done many *in vivo* experiments on animals to better understand how the body reacts to a TBI and to explore better treatment [5]. One of the earliest *in vivo* TBI test was done on large animals (cats, dogs, and monkeys) because their similarly sized brain gave a better comparison to humans' when looking at "intracranial pressure, brain tissue oxygen content, and cerebral blood flow" [6]. However, many disadvantages such as more

complex surgical procedures, longer life spans, and more expensive housing and imaging facilities for these large animals made rodent tests the most popular and widely used [5]. Four main TBI models on rodents include: the first is the fluid percussion injury model which injects fluid directly on the brain to observe results of brain deformation; the controlled cortical impact injury model causes a mechanical deformation through an electromagnetic device; the weight drop-impact acceleration model drops a weight at different heights onto exposed skull; lastly, the blast injury model replicates explosion blast forces which cause the TBIs commonly suffered by servicemen and women [7].

1.03 Current Research–*In Vitro* Testing

Despite the extensive *in vivo* research available, there is still a gap in understanding how the brain responds on a cellular level. *In vitro* testing is vital to understand this better, and the tissue engineering field has determined that hydrogels are ideal to expand this research. One of the best properties of hydrogels that make them so important for studying TBIs is that they are easily parametrizable to have different mechanical properties through changing the temperature of fabrication, concentrations of solutions, and crosslinkers. Hydrogels are made up of a 3D network of hydrophilic polymers that swell and can hold a large amount of water while maintaining their structure [8]. This is a result of the addition of a cross-linker that can chemically or physically cross-link the individual polymer chains [8]. Since hydrogels have a high-water content and viscoelastic properties, they can be used to imitate brain matter and replicate the extracellular matrix of the brain [9].

1.04 Group 18 BME Senior Design Project (2021-2022)

Currently, there are no accurate *in vitro* models of brain matter that allow scientists to better understand and study how the brain matter and the cells within responds to a TBI. More

specifically, the limitation on the modeling of TBIs results in limited understanding of the damage that brain injuries have on the cellular level. To address this, Group 18 BME Senior Design aimed to design a hydrogel that accurately replicates the mechanical properties of brain matter under conditions consistent with cell culturing. This is to provide an accurate *in vitro* brain model to use to better understand the impact TBIs have on the cellular level. After conducting an extensive literature review on existing hydrogels and comparing their mechanical properties of the brain, four different hydrogels were fabricated with varying concentrations of alginate and gelatin. After successfully creating stable hydrogels that would hold for up to 5 days, rheology testing and SEM imaging was done to understand the mechanical properties and microstructure of these hydrogels and how they were affected by changing alginate and gelatin concentrations.

The Senior Design project chose to create alginate and gelatin hydrogel composites due to the literature and an experiment performed by Distler, et al. that demonstrated that these hydrogel hybrids could replicate similar mechanical properties to porcine brain [10]. The asymmetry and nonlinear behavior of alginate combined with the linear response of gelatin mimics the linear and nonlinear properties of brain. Additionally, alginate and gelatin are biocompatible and would allow the implementation of cells so future projects can observe the impacts on the seeded cells when inflicted with blunt forces.

1.05 SEM Pore Analysis

To further expand on the senior design project, this Honors Thesis analyzes the SEM imaging of the hydrogels to investigate the porosity of each hydrogel composition and how the variation of the gelatin and the alginate may affect the pore sizes. The interconnectivity of the pores is a direct factor in the mechanical and biological properties of the hydrogel scaffolds. The architecture of the hydrogels allows for “cell migration, proliferation, and extracellular matrix

deposition [11].” The size of the pores directly affects transport within the hydrogel and therefore the outcomes following cell implantation. Porosity is important for cell-cell interaction, migration, proliferation, and exchange of oxygen, nutrients, and waste materials in and out of the hydrogels [12]. Mean pore diameter and total pore volume (porosity) are two physical properties that are closely researched through SEM imaging [11]. When analyzing the samples, I will be looking especially at pore size and verifying that the pore diameters are no smaller than 4 μm and no larger than 100 μm which is the range for a human neuron [13]. Pore sizes that are too small would block neuron migration [14]. Additionally, the porosity is inversely proportional to stiffness of the hydrogels, meaning that a hydrogel with high porosity makes it less stiff [15]. With a high porosity, cells can migrate and proliferate by adhering to the fibers within the pores and easily connecting with neighboring cells [16].

By analyzing the porosity of the hydrogels created by the Senior Design group through comparing average pore diameter, a prediction will be developed on how cells will thrive for future projects that incorporate cells. The results will also be compared to the mechanical properties that were gathered to confirm the relationship between porosity, stiffness, and cell viability potential in each of the fabricated hydrogels.

2. Materials and Methods

2.01 Fabrication of Hydrogels

The fabrication of the hydrogels for SEM imaging and analysis was conducted as part of Group 18 BME Senior Design project. The bill of materials (BOM) is listed in Table 1. Bill of Materials. which lists all the materials needed to fabricate the hydrogels without adding standard lab equipment.

Table 1. *Bill of Materials.*

Description	**Source/Catalog #**
Gelatin (Gel Strength 300, Type A)	Sigma-Aldrich G1890
Sodium Alginate	Sigma-Aldrich W201502
TI Transglutaminase	Modernist Pantry 1203-50
Calcium Chloride Dihydrate	Fisher Scientific C79-500
Phosphate Buffered Saline Solution (PBS)	Sigma-Aldrich D8537
Deionized Water	Sigma-Aldrich 8.48333

The protocol for the fabrication of the four different concentrations is as follows:

1. Turn on hot plate/stirrer to 80ºC and 200rpm.
2. Create 0.1 M $CaCl_2$ solution.
    a. Mix 50mL dH_2O and 0.555g of $CaCl_2$ in a conical tube.
    b. Place in 80ºC water bath and vortex until fully incorporated.
    c. Make sure to store in fridge once homogenous solution is made.
3. Create 10% TG solution.
    a. Mix 50mL PBS and 5g TG in a conical tube.
    b. Place in 80ºC water bath and slowly invert (do not vortex).
    c. Make sure to store in fridge once homogenous solution is made.
4. Make the proper alginate and gelatin solution following Table 2 below.

Table 2. Amounts needed to create alginate and gelatin solutions.

%W/V	**Solute Amount (g)**	**Solvent Amount (mL)**
Alginate 1% Solution	0.05g alginate	4.95 mL PBS
Alginate 2% Solution	0.10g alginate	4.90 mL PBS
Gelatin 1% Solution	0.05g gelatin	4.95 mL PBS

Gelatin 2% Solution	0.10g gelatin	4.90 mL PBS

5. Mix solutions depending on what concentration hydrogels you want to make.
    a. Ex: for 1% ALG/1% GEL, mix 5mL of the 2% ALG solution and 5mL of the 2% GEL solution to create 10mL of a 1% ALG/1% GEL solution.
6. Pipette 500µL of solution into the bottom of wells.
7. Let set for 5 mins before spraying with $CaCl_2$ then let rest for 15 mins.
8. Use spatula to scrape around the edges of the wells before adding 500µL of $CaCl_2$ to each well. Lift hydrogel to ensure the $CaCl_2$ surrounds the gel.
9. Let rest for 45 more mins at room temperature.
10. Aspirate off the $CaCl_2$ solution and use a spatula to remove the hydrogels.
11. Place the hydrogels in 60mm petri dishes and add 3-5mL of TG solution to each petri dish.
12. Place in incubator for 24 hours.
13. After 24 hours, remove TG and replace it with PBS. Place back into the incubator.

2.02 Preparation of Hydrogels for SEM Imaging

Conventional SEM cannot have wet samples in the electron beam chamber since "vaporized water molecules would interfere with the primary or secondary electron beam" [16]. As such we prepared the samples for proper SEM imaging as outlined below.

Fabricated hydrogels were cryofrozen in a liquid nitrogen bath to maintain the internal microstructure of the hydrogels. Next, they were removed and cross-sectioned with a razor blade in multiple pieces. These pieces were then placed back into the liquid nitrogen bath for about 5-10 minutes while continuously stirring with a spatula until fully frozen. The cross-sectioned pieces were collected in a 15mL conical tube without the cap and placed in a lyophilizer container. They

were sealed in a lyophilization chamber for 48 hours to dehydrate and remove all moisture from the samples while maintaining the microstructure [18]. The lyophilizer removes any moisture so that they can be placed in the vacuum environment of the sputter coater. Any moisture would prevent the sputter coater to coat the sample uniformly. All samples from the four concentrations were treated in the same way and this process is shown in Figure 1.

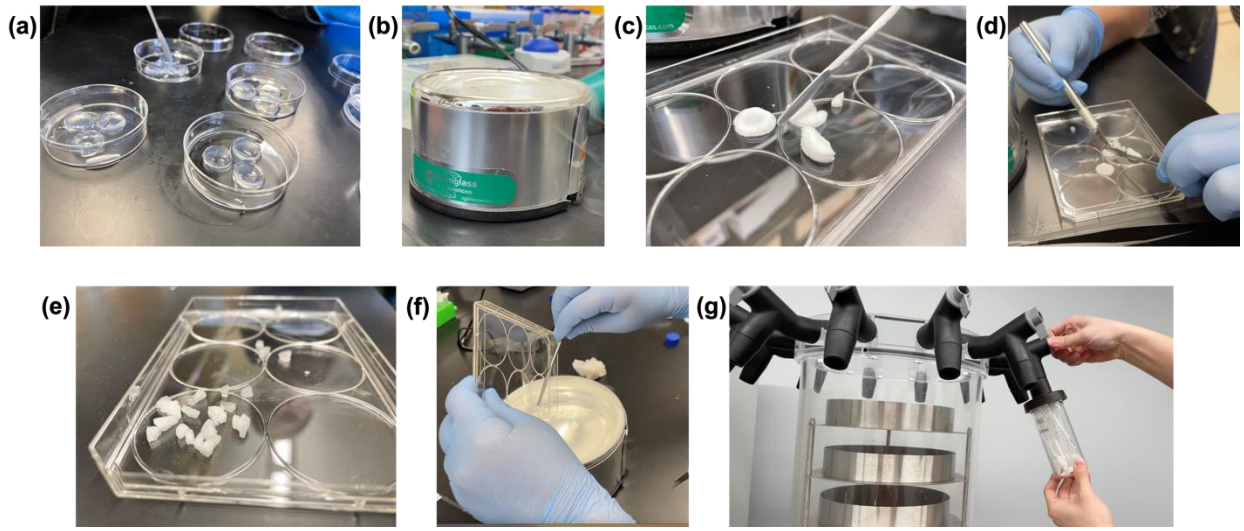

Figure 1. *Preparation of samples for lyophilization. (a) Each concentration of hydrogels was fabricated and crosslinked. (b) Hydrogel disc was placed in liquid nitrogen bath. (c) Discs were removed. (d) Samples were cut to reveal the interior. (e) Image of cut hydrogels. (f) The cut sections were placed in bath again. (g) Fully frozen samples were put in lyophilizer for 48 hours.*

After 48 hours, the dehydrated cross-sections of the hydrogel were mounted on metal stub using sticky carbon tape (which increases conductivity) for SEM imaging. The samples were laid ensuring the cross section of the hydrogel was facing upward to allow the SEM to image the inside structure of the hydrogel. The stub was then inserted in a sputter coater and the samples were sputter coated with a 15nm thick layer of gold-palladium (Au/Pd). Coating the samples is vital before SEM imaging because it prevents charging of the hydrogel and applies a conductive material allowing the electrons from the SEM beam to coat the surface and increase the signal to noise ratio [18]. The mount was then inserted in the SEM machine and imaged. This process is shown in Figure 2.

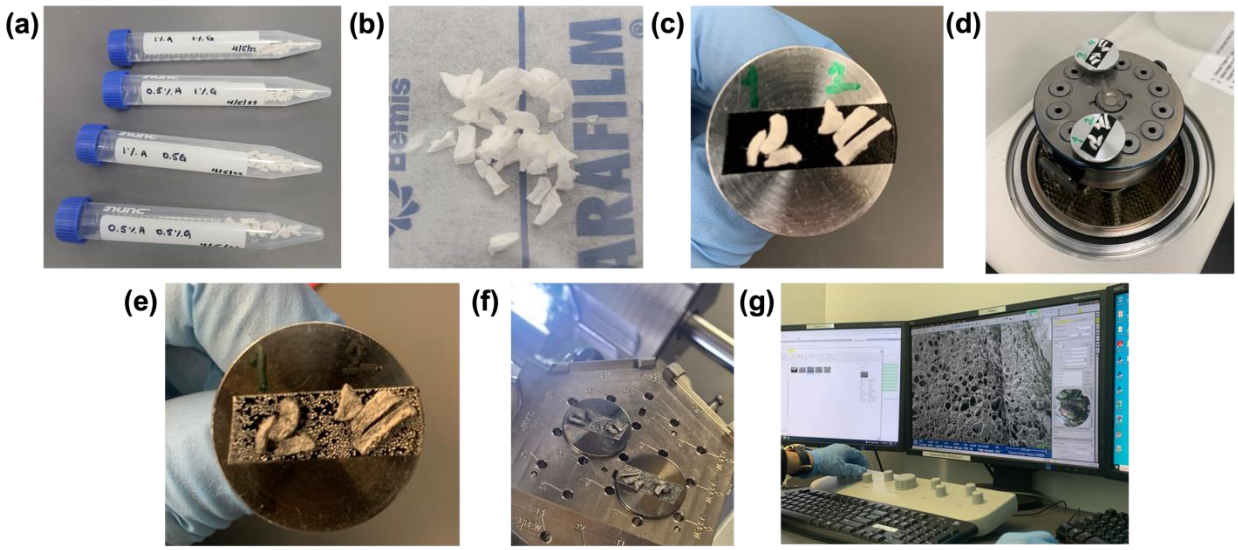

Figure 2. *Preparation of samples for SEM imaging. (a) Dehydrated samples removed from lyophilizer. (b) Dehydrated samples. (c) Samples mounted on carbon tape with interior cross-section facing upwards. (d) Mounted samples inserted in the sputter coater. (e) Sputter coated samples. (f) Samples mounted into SEM machine. (g) Samples were imaged.*

For each concentration, a macro image at 150x magnification and a minimum of six micro images at 500x magnification were taken throughout the 3-4 samples. The resulting SEM images are shown in Figure 4. Images were taken from different cross-sectional hydrogel samples. Each cross section was further imaged at six different regions. These images were then analyzed via *ImageJ* for pore size measurements for different samples.

2.03 Analysis of SEM Images

Each of the SEM images were uploaded to *ImageJ*, a java-based image processing program developed at the National Institutes of Health and the Laboratory for Optical and Computational Instrumentation. For each image, the measurement tool was calibrated using the scale at the bottom of each SEM image. Next, measurements of the diameter of as many pores as possible were collected for each image and concentration. Averages of the diameter size were taken for each image and concentration as well. The process is shown in Figure 3 and the resulting images are shown in Figures 5-8.

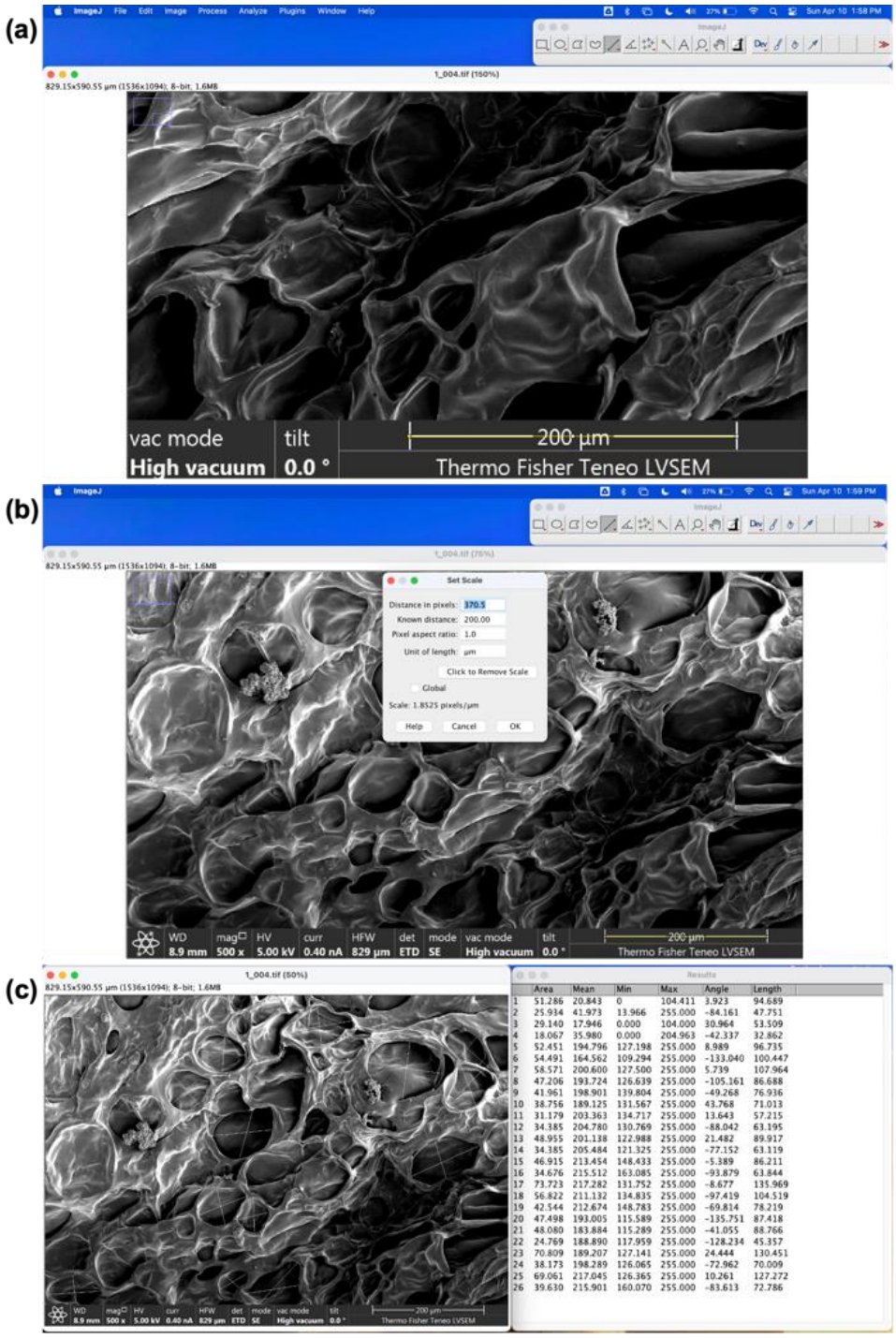

Figure 3. *Analysis of SEM images using ImageJ. (a) Straight line measurement of the scale bar in pixels. (b) Conversion of the pixel measurement to the known length of the bar in um. (c) Collection of pore diameters lengths before transferred to excel document.*

3. Results

3.01 SEM Imaging

SEM images were taken at a macro level at 150x magnification and a micro level at 500x magnification with each of the four concentrations of hydrogels. This is shown in Figure 4.

Qualitatively, these images show a trend that with an increase in the concentration of alginate and gelatin, the porosity decreases. This is seen with the two “extremes” of 0.5%ALG/0.5%GEL, the lowest concentration, which has much larger pores than 1.0%ALG/1.0%GEL, the highest concentration. With higher concentrations, meaning more of the alginate and gelatin solution added, the hydrogels appear to be much denser and compact making smaller pores. Additionally, the 0.5%ALG/1.0%GEL gels visually have smaller pores than the 1.0%GEL/0.5%ALG gels suggesting that the increase in gelatin directly decreases the pore size.

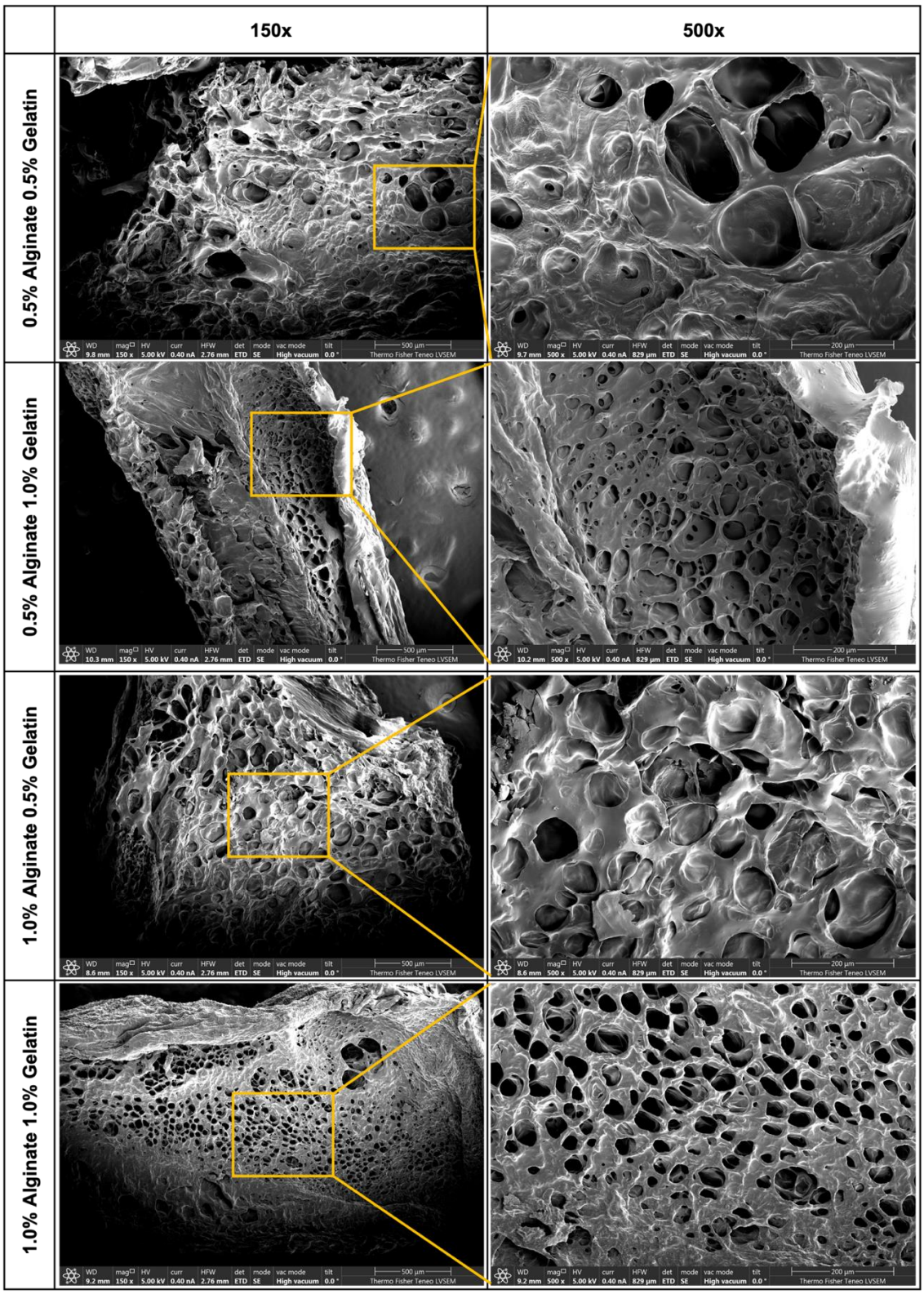

Figure 4*. SEM images through the cross-section for each composition of alginate and gelatin hydrogels. Images in the left column show the morphology of the hydrogels at 150x. The boxed region of interest is further magnified at 500x on the right to show the pore*

3.02 SEM Imaging Measurements

All SEM images at 500x magnification are shown at the four concentrations in Figures 5-8. A minimum of six images were taken at each concentration to increase the variety of pores seen throughout the hydrogel and provide a more accurate average. In total, a couple hundred pore diameter measurements were taken among those images at each concentration. Through *ImageJ,* measurements were taken on as many pores as possible. The white lines across the pores on each of the images in Figures 6-9 indicate all the spots that measurements were recorded and collected through *ImageJ*. Keeping the lines helped prevent measuring the same pore multiple times and provides a visual on the vast number of measurements taken. Each of these values recorded from each of the white lines are listed in Tables 4-7 located in the appendix.

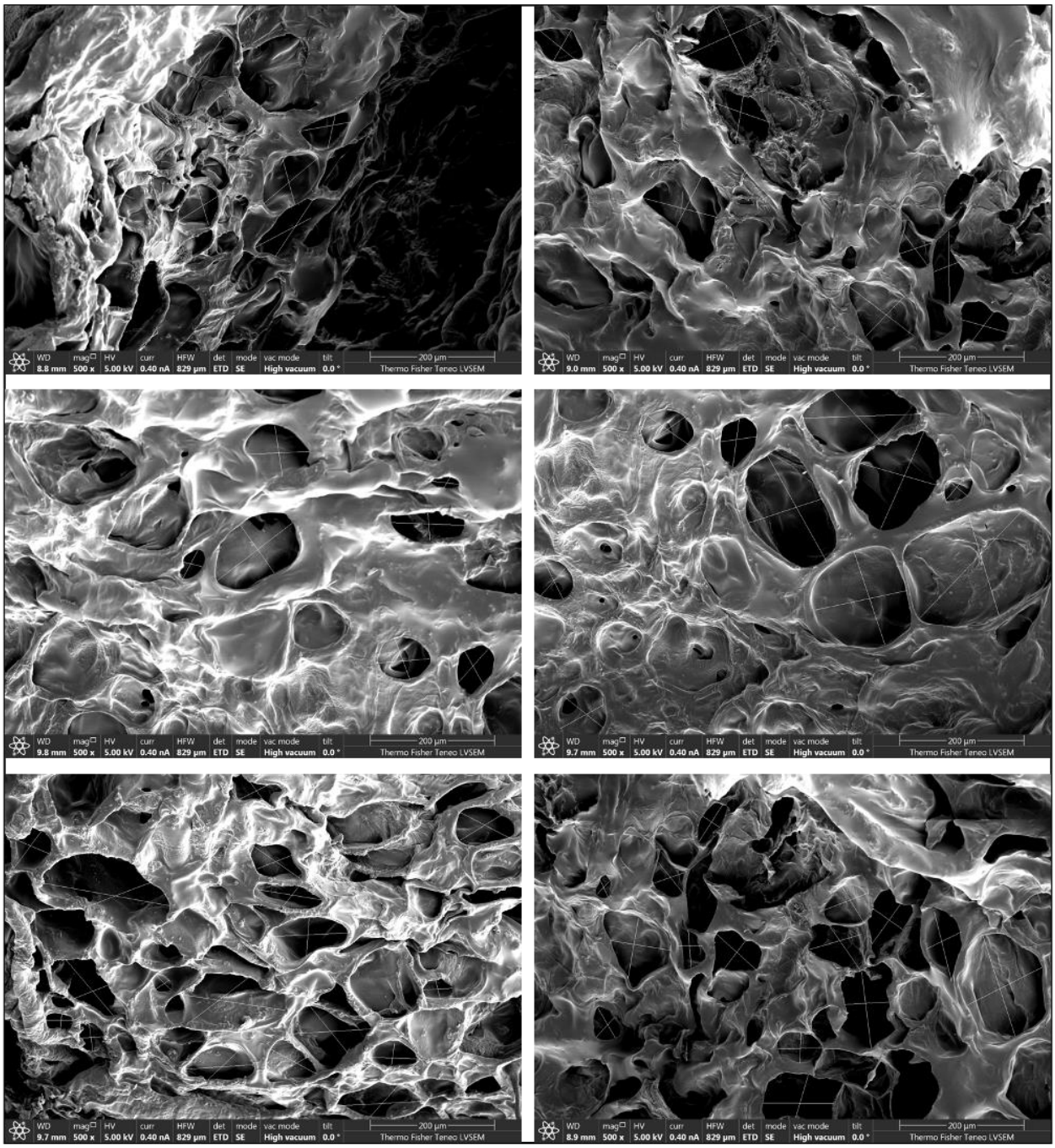

Figure 5*. 0.5% Alginate 0.5% Gelatin images at 500x magnification. Pore size measurement locations are shown with white lines across the diatmeters of the pores.*

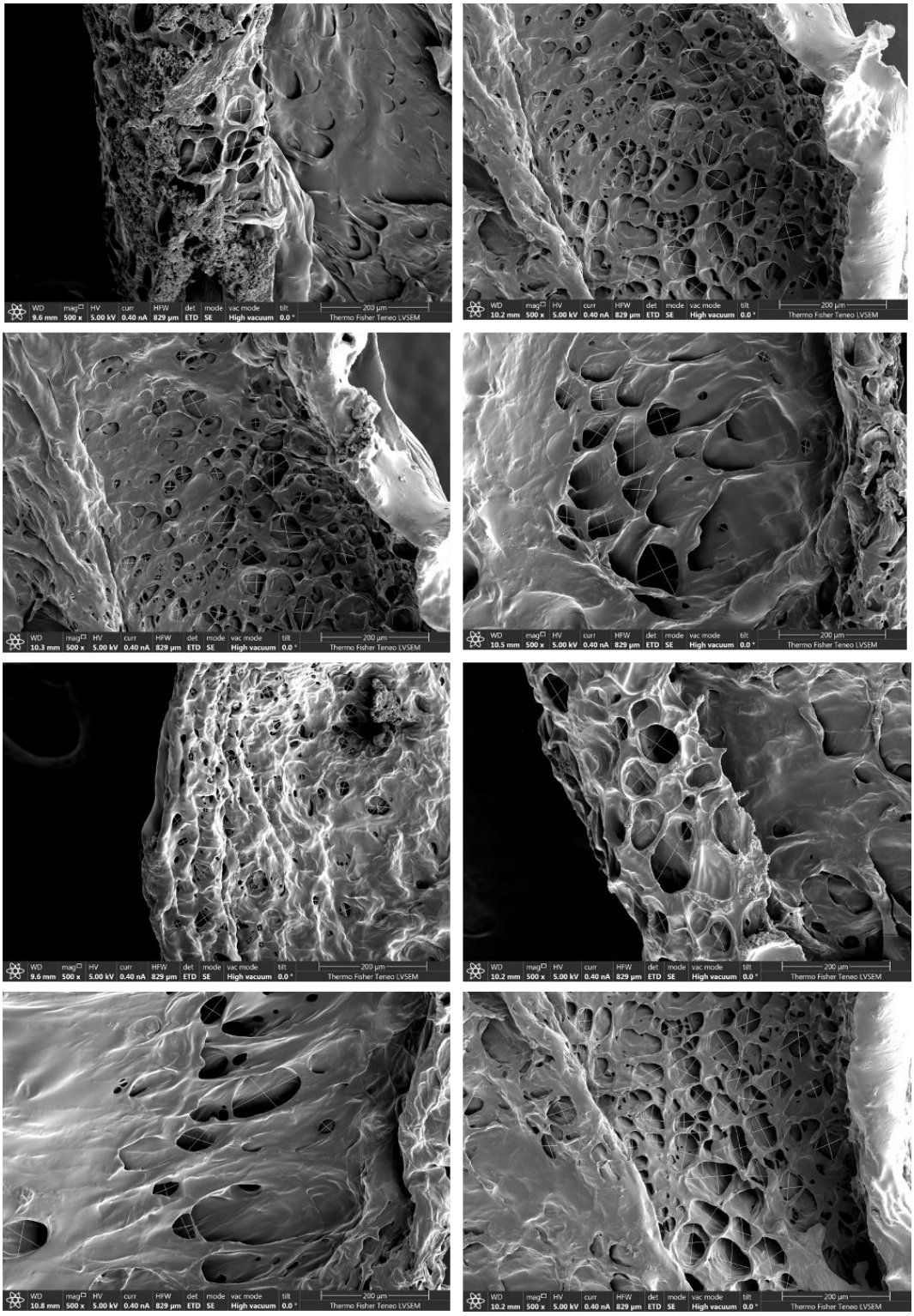

Figure 6*. 0.5% Alginate 1% Gelatin images at 500x magnification. Pore size measurement locations are shown with white lines across the diatmeters of the pores.*

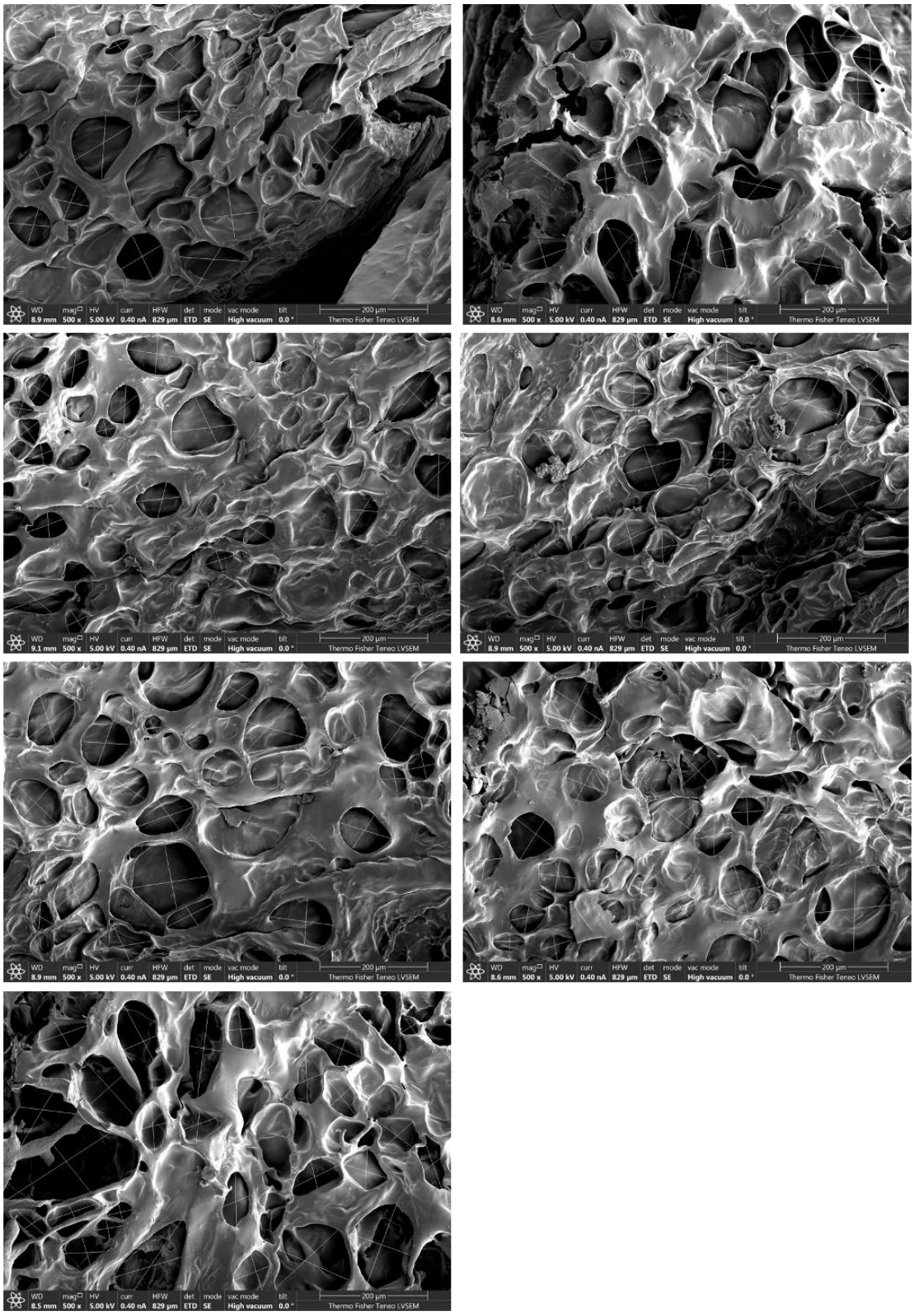

Figure 7*. 1% Alginate 0.5% Gelatin images at 500x magnification. Pore size measurement locations are shown with white lines across the diatmeters of the pores.*

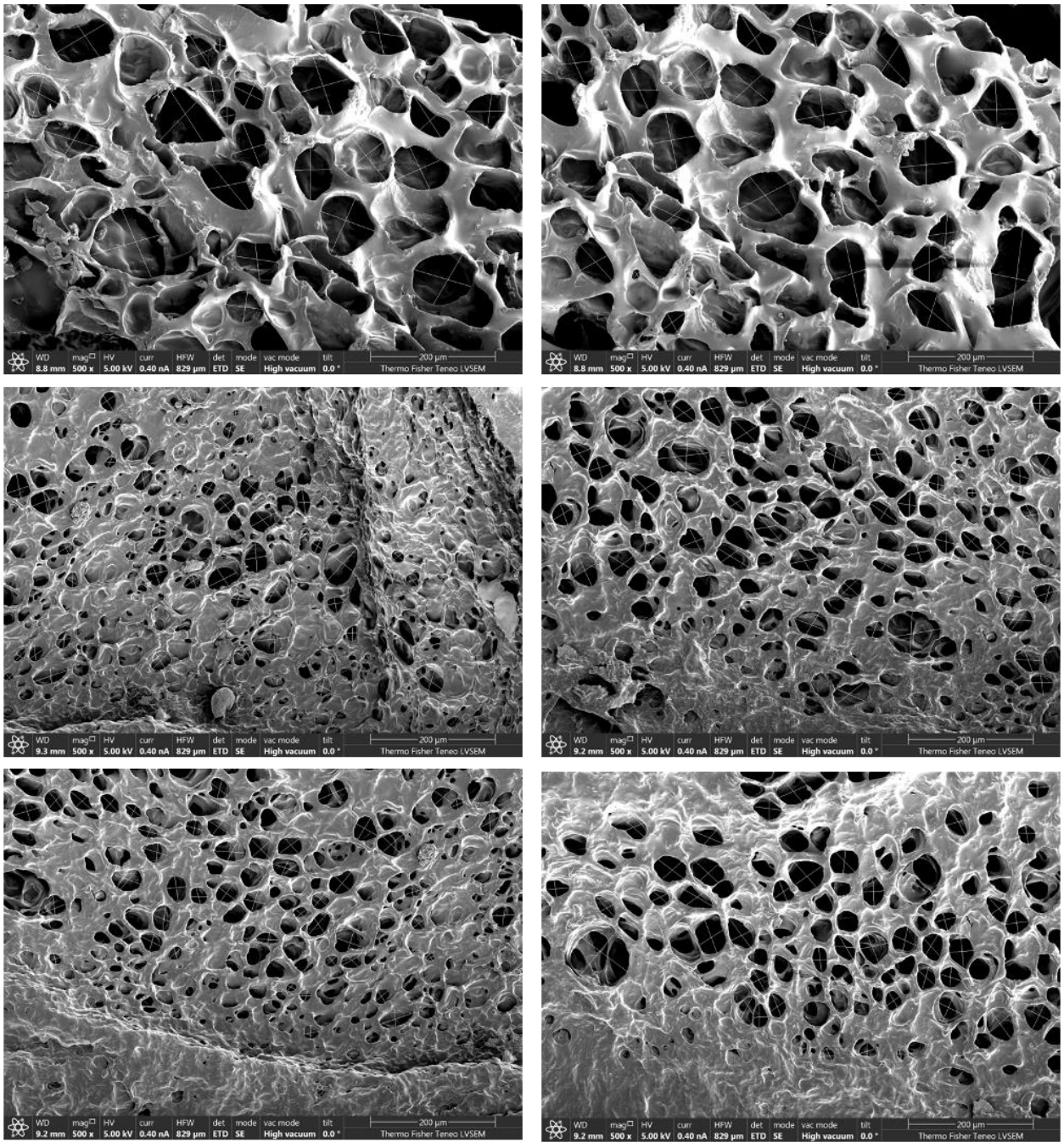

Figure 8. *1.0% Alginate 1.0% Gelatin images at 500x magnification. Pore size measurement locations are shown with white lines across the diatmeters of the pores.*

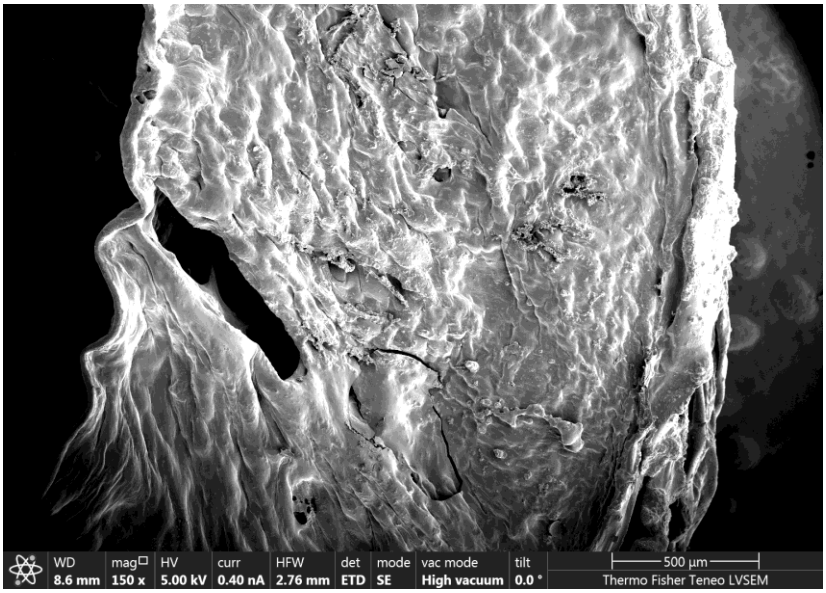

Figure 9. *0.5% Alginate 0.5% Gelatin at 150x magnification. Due to the lack of pores seen, this is an image of the outer surface of the hydrogel. There is no porosity because of the uniform crosslinking from the $CaCl_2$ and TG that occurred directly on the surface.*

3.03 Pore Size Averages

The quantitative results of average pore size for each of the four concentrations is shown in Table 3 and illustrated in Figure 10. 0.5% ALG/0.5%GEL has the largest average pore size at 84.89 µm while 0.5% ALG/1% GEL and 1% ALG/1% GEL are comparably the smallest at 38.37 µm and 41.31 µm respectively. There is a statistical significance difference in pore size between 0.5% ALG/0.5% GEL, at 84.89 µm, and 0.5% ALG/1% GEL, at 38.37 µm, as well as between 0.5% ALG/0.5% GEL and 1% ALG/1% GEL, at 41.31 µm, directly showing that an increase in gelatin specifically decreases the average pore size.

Table 3. *Average pore diameter for each concentration.*

0.5% Alginate 0.5% Gelatin	**0.5% Alginate 1% Gelatin**	**1% Alginate 0.5% Gelatin**	**1% Alginate 1% Gelatin**
84.89 µm	38.37 µm	77.22 µm	41.31 µm

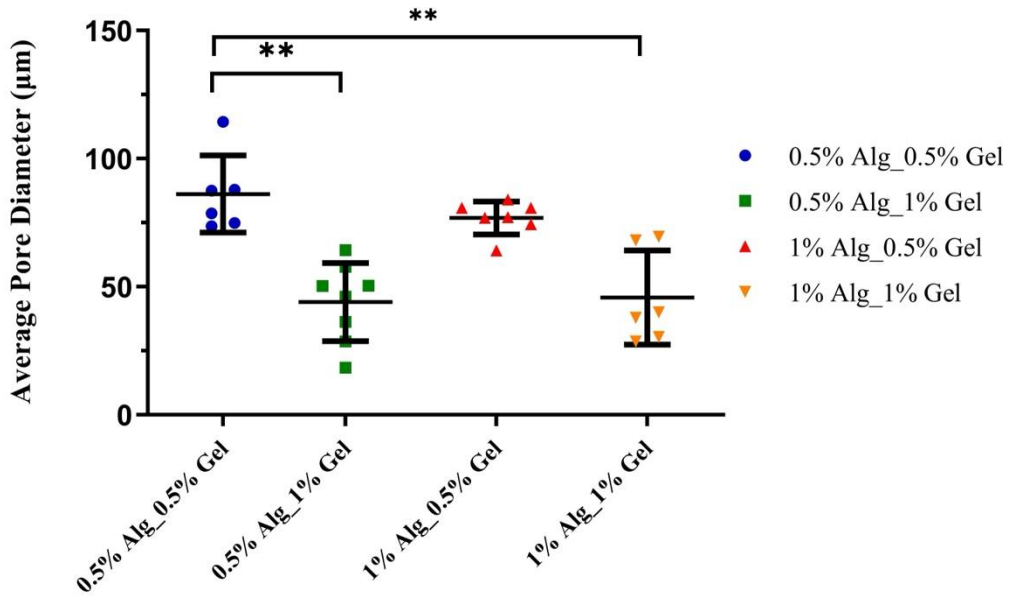

Figure 10. *Graph comparing the average pore diameter in µm of each concentration. (** p<0.0001).*

4. Discussion

The SEM images confirmed the porous structure of the hydrogels for all compositions of gelatin and alginate. This shows that all the hydrogels will allow for proper cell encapsulation. This is seen at all concentrations and is obvious when comparing them to an image of a hydrogel's surface in Figure 9. Additionally, when looking at the macro images of each concentration at 150x magnification, it is obvious that 1.0% alginate/1.0% gelatin hydrogels have smaller pore sizes than the 0.5% alginate/0.5% gelatin hydrogels because they are much denser and stiffer. This is also reflected in the rheology results of Group 18 BME Senior Design project, and we can interpret that increasing the concentration or gelatin and alginate not only increases the stiffness of the hydrogels but also decreases the porosity of hydrogels.

When looking directly at the calculated averages of pore diameter for each of the concentrations, the trend suggests that gelatin controls the porosity since the difference between 0.5% ALG/0.5% GEL and 0.5% ALG/1% GEL is statistically significant. The change in

concentration affecting the pore size is obvious when comparing 0.5% ALG/0.5% GEL with an average pore size of 84.89 µm versus 1% ALG/1% GEL which has an average pore size of 41.31 µm. When comparing the 1% ALG/1% GEL with 0.5% ALG/1% GEL which has an average pore diameter of 38.37 µm, it shows that it is the gelatin may affect the pore size difference. We think this happens because gelatin binds between the alginate fibers and fill the pores. Further tests are needed to confirm this trend and can be a part of future directions. However, the presence of the gelatin would allow for cell adhesion and proliferation because alginate along does not have the RGD peptides for cell adhesion.

All the values gathered were done with a degree of randomness to increase the validity of the results. First, three hydrogel discs of each concentration were cut in many different sections and mixed into one 15mL conical tube. Then, 3-4 samples were randomly chosen for each concentration to me SEM imaged. Finally, when measuring the pore sizes with *ImageJ*, pores were randomly selected throughout all the images. To improve on this project, the SEM imaging should be conducted blind, and the randomness could be improved by increasing the number of samples imaged and number of pores measured.

5. Conclusion and Future Work

Overall, this study confirmed that the hydrogels created by Group 18 BME Senior Design project are porous and would support cell life and proliferation and that the concentration of gelatin is directly proportional to pore size. By creating hydrogels with 4 different concentrations, cryofreezing them in a liquid nitrogen bath to preserve their structure, lyophilizing them for 48 hours to freeze dry them and remove all moisture, and finally imaging them through SEM, this project paved the way for future work in implanting the hydrogels with neuronal cells and eventually conduct impact testing to better understand TBIs. This quantification of the pore sizes

also provides interesting insights into how the composition of the hydrogel microstructure changes with varying concentration of alginate and gelatin and how this may further affect the cellular interactions with the hydrogel material.

6. Acknowledgements

I would like to begin with thanking Dr. Fayekah Assanah, my BME Senior Design and Honors Thesis advisor for her countless hours of support and teaching to help me better understand hydrogels, SEM imaging, and importance of research overall.

Next, I would like to thank Dr. Wuxia Zhang and Dr. Yupeng Chen for allowing me to use their lab and materials in preparing our samples for lyophilization. Thank you also to Dr. Baris Yavas for donating his time to image all my samples and sharing his knowledge.

Lastly, I want to thank Group 18 BME Senior Design group members (Olivia Rice, Sydney Griger, Leah Faber, Leah Sobotka, and Kristen Soldau) for supporting my honors thesis by helping create hydrogels and navigating through the challenges of Senior Design together.

Thank you, everyone!

7. References

[1] Yun Ng. (2019). Traumatic Brain Injuries: Pathophysiology and Potential TherapeuticTargets. *Frontiers in Cellular Neuroscience.*, *13*.

[2] Centers for Disease Control and Prevention. (2021, May 12). *Get the facts about tbi*. Centers for Disease Control and Prevention. Retrieved September 22, 2021, from https://www.cdc.gov/traumaticbraininjury/get_the_facts.html.

[3] Warden, Deborah MD Military TBI During the Iraq and Afghanistan Wars, Journal of Head Trauma Rehabilitation: September 2006 - Volume 21 - Issue 5 - p 398-402

[4] Dixon, K. J. (2017). Pathophysiology of Traumatic Brain Injury. *Physical Medicine and Rehabilitation Clinics of North America, 28*(2), 215-225. https://doi.org/10.1016/j.pmr.2016.12.001

[5] Xiong, Y., Mahmood, A., & Chopp, M. (2013). Animal models of traumatic brain injury. *Nature reviews. Neuroscience*, *14*(2), 128–142. https://doi.org/10.1038/nrn3407

[6] Shah, Ekta & Gurdziel, Katherine & Ruden, Douglas. (2019). Mammalian Models of Traumatic Brain Injury and a Place for Drosophila in TBI Research. Frontiers in Neuroscience. 13. 10.3389/fnins.2019.00409.

[7] Shah, Ekta & Gurdziel, Katherine & Ruden, Douglas. (2019). Mammalian Models of Traumatic Brain Injury and a Place for Drosophila in TBI Research. Frontiers in Neuroscience. 13. 10.3389/fnins.2019.00409.

[8] Bahram, M., Mohseni, N., & Moghtader, M. (2016). An Introduction to Hydrogels and Some Recent Applications. In (Ed.), Emerging Concepts in Analysis and Applications of Hydrogels. IntechOpen. https://doi.org/10.5772/64301

[9] Kornev, V. A., Grebenik, E. A., Solovieva, A. B., Dmitriev, R. I., & Timashev, P. S. (2018). Hydrogel-assisted neuroregeneration approaches towards brain injury therapy: A state-of-the-art review. *Computational and structural biotechnology journal*, *16*, 488–502. https://doi.org/10.1016/j.csbj.2018.10.011

[10] Distler, T., Schaller, E., Steinmann, P., Boccaccini, A. R., & Budday, S. (2020). Alginate-based hydrogels show the same complex mechanical behavior as brain tissue. *Journal of the mechanical behavior of biomedical materials*, *111*, 103979. https://doi.org/10.1016/j.jmbbm.2020.103979

[11] Somo, S. I., Akar, B., Bayrak, E. S., Larson, J. C., Appel, A. A., Mehdizadeh, H., Cinar, A., & Brey, E. M. (2015). Pore Interconnectivity Influences Growth Factor-Mediated Vascularization in Sphere-Templated Hydrogels. *Tissue engineering. Part C, Methods*, *21*(8), 773–785. https://doi.org/10.1089/ten.TEC.2014.0454

[12] Leal-Egaña, A., Braumann, U. D., Díaz-Cuenca, A., Nowicki, M., & Bader, A. (2011). Determination of pore size distribution at the cell-hydrogel interface. *Journal of nanobiotechnology*, *9*, 24. https://doi.org/10.1186/1477-3155-9-24

[13] Cotter D, Mackay D, Landau S, Kerwin R, Everall I. Reduced Glial Cell Density and Neuronal Size in the Anterior Cingulate Cortex in Major Depressive Disorder. *Arch Gen Psychiatry.* 2001;58(6):545–553. doi:10.1001/archpsyc.58.6.545

[14] Julian George, Chia-Chen Hsu, Linh Thuy Ba Nguyen, Hua Ye, Zhanfeng Cui, Neural tissue engineering with structured hydrogels in CNS models and therapies, Biotechnology Advances, Volume 42, 2020, 107370, ISSN 0734-9750, https://doi.org/10.1016/j.biotechadv.2019.03.009.

[15] Hwang, C. M., Sant, S., Masaeli, M., Kachouie, N. N., Zamanian, B., Lee, S. H., & Khademhosseini, A. (2010). Fabrication of three-dimensional porous cell-laden hydrogel for tissue engineering. *Biofabrication*, *2*(3), 035003. https://doi.org/10.1088/1758-5082/2/3/035003

[16] Annabi, N., Nichol, J. W., Zhong, X., Ji, C., Koshy, S., Khademhosseini, A., & Dehghani, F. (2010). Controlling the porosity and microarchitecture of hydrogels for tissue engineering. *Tissue engineering. Part B, Reviews*, *16*(4), 371–383. https://doi.org/10.1089/ten.TEB.2009.0639

[17] Podhorská B, Vetrík M, Chylíková-Krumbholcová E, Kománková L, Rashedi Banafshehvaragh N, Šlouf M, Dušková-Smrčková M, Janoušková O. Revealing the True Morphological Structure of Macroporous Soft Hydrogels for Tissue Engineering. *Applied Sciences*. 2020; 10(19):6672. https://doi.org/10.3390/app10196672

[18] Lee, K. Y., & Mooney, D. J. (2012). Alginate: properties and biomedical applications. Progress in polymer science, 37(1), 106–126. https://doi.org/10.1016/j.progpolymsci.2011.06.003

[19] Höflinger, Gisela. “Brief Introduction to Coating Technology for Electron Microscopy.” *Science Lab | Leica Microsystems*, Leica Microsystems, 28 Aug. 2013, https://www.leica-microsystems.com/science-lab/brief-introduction-to-coating-technology-for-electron-microscopy/

8. Appendix

Table 4*. Collection of pore diameter measurements for each image of 0.5%Alginate/0.5% Gelatin.*

500x	1_003	1_004	1_005	1_006	1_007	1_009	
	Length	Length	Length	Length	Length	Length	Average (um)
1	153.088	128.263	169.692	156.835	78.334	129.866	84.889056
2	94.192	90.095	134.287	150.982	68.819	60.695	
3	84.617	77.267	113.972	194.049	113.006	77.868	
4	71.68	57.868	62.057	122.571	76.604	35.47	
5	73.486	122.157	87.503	77.766	77.3	206.445	
6	59.538	89.084	57.237	57.712	52.52	111.032	
7	117.377	54.113	55.128	173.512	52.52	116.556	
8	43.947	61.647	43.35	125.069	108.994	59.924	
9	55.867	156.05	97.929	185.019	103.105	125.094	
10	32.252	103.347	97.214	112.873	148.353	93.37	
11	82.029	59.724	61.981	82.721		44.721	
12	99.553	73.684	37.94	78.523		37.9	
13	42.442	75.968	66.649	69.915		43.243	
14	22.063	93.724	122.892	60.305		23.3	
15		117.144	72.186	237.16		168.333	
16		41.702	72.089	164.046		116.541	
17			47.746	43.971		110.494	
18			114.364	37.97		72.265	
19			70.656	79.814		92.065	
20			49.879	78.647		60.427	
21			62.47			108.949	
22			28.371			41.957	
23			32.484			74.162	
24			72.166			61.04	
25			31.72			78.615	
26			86.959			89.451	
27			87.207			47.644	
28			78.066			30.678	
29			60.299			135.318	
30						68.142	
31						55.117	
32						42.921	
33						32.88	
34						25.336	
35						82.958	
36						72.879	

Table 5*. Collection of pore diameter measurements for each image of 0.5% Alginate/1.0% Gelatin*

500x	1_001	1_002	1_003	1_004	1_005	1_006	1_009	1_010	
	Length	Length	Length	Length	Length	Length	Length	Length	Average (um)
1	36.757	45.073	77.511	81.27	82.944	51.673	26.744	47.401	38.37324768
2	63.367	53.341	71.459	71.354	103.226	25.497	21.581	32.261	
3	33.096	66.37	68.189	70.428	72.573	46.58	51.089	62.404	
4	31.197	33.413	75.899	73.184	46.675	41.868	44.761	32.129	
5	35.057	46.987	76.465	127.761	35.197	61.795	39.784	62.134	
6	38.275	30.778	43.871	74.635	39.493	60.01	24.753	70.104	
7	46.229	58.84	86.7	78.063	55.741	135.259	21.79	44.8	
8	40.757	56.716	60.75	68.22	63.614	76.299	11.403	26.376	
9	57.861	66.152	46.09	80.3	103.249	33.761	20.312	45.866	
10	47.488	57.818	50.974	43.639	70.594	26.371	14.271	54.122	
11	65.868	55.804	68.335	44.542	62.835	64.406	9.73	43.797	
12	62.144	49.744	52.794	34.911	53.207	38.743	8.391	29.259	
13	61.997	45.057	27.012	54.227	68.98	70.205	10.27	51.677	
14	56.686	34.4	33.368	47.929	45.524	76.181	9.189	43.727	
15	17.284	40.28	30.273	47.549	45.189		20.117		
16	19.946	48.363	23.85	30.705	40.091		14.189		
17	25.882	45.306	33.538		14.054		11.025		
18	26.15	33.163	31.867		17.432		6.509		
19	41.986	43.142	38.387		62.049		25.238		
20	38.483	39.751	30.769		44.235		13.95		
21	19.822	63.923	53.77		26.619		12.444		
22	55.567	39.784	49.701		17.607		9.864		
23	48.962	54.659	49.677		25.497		22.587		
24	24.36	33.726	28.075		14.764		17.895		
25	28.464	57.694	67.838				22.496		
26	16.72	51.309	43.36				23.468		
27	17.385	35.778	53.973				27.562		
28	30.595	35.135	51.959				17.17		
29	32.417	34.208	52.813				17.204		
30	20.514	33.413	40.489				9.923		
31	16.885	46.703	35.953				14.096		
32	26.172	32.991	43.911				12.849		
33	26.765	18.639	55.995				8.915		
34	21.347	21.109	37.791				5.643		
35	21.462	29.194	73.82				15.759		
36	16.253	22.287	58.839				11.403		

37	15.333	41.73	58.422				9.578		
38	22.162	33.092	56.016				15.713		
39	15.781	28.654	50.214				16.792		
40	19.953	25.686	54.307				9.189		
41	21.805	77.802	50.437				12.479		
42	44.532	55.613	48.918				18.45		
43	32.223	25.331	50.205				34.611		
44	9.643	15.298	49.489				31.426		
45	8.709	37.644	32.59				45.665		
46	18.829	33.774	32.181				35.647		
47	14.803	51.694	55.19				28.066		
48	24.354	43.179	47.337				23.268		
49	20.584	30.816	88.298				18.67		
50	17.284	32.088	34.332				18.171		
51	21.671	43.043	42.522				15.26		
52	25.769	28.725	25.832				10.398		
53	23.775	15.898	62.282				17.599		
54	9.643	15.222	72.02				7.272		
55	7.624	7.739	43.212				9.331		
56	14.595	9.967	40.64				11.941		
57	10.741	44.338	39.001				14.147		
58	11.612	20.689	42.205				10.44		
59	9.212	21.081	54.625						
60		20.196	51.421						
61		18.041	51.959						
62		18.927	53.417						
63		28.093	45.804						
64		21.322	28.656						
65		29.109	65.919						
66		18.41	68.275						
67		29.984							
68		26.93							
69		20							
70		32.504							
71		33.255							
72		21.709							

Table 6*. Collection of pore diameter measurements for each image of 1.0% Alginate/0.5% Gelatin*

500x	1_001	1_002	1_003	1_004	1_005	1_006	1_007	
	Length	Length	Length	Length	Length	Length	Length	Average (um)
1	154.412	149.224	109.082	109.082	113.901	84.793	88.214	77.22423423
2	116.779	141.891	80.112	80.112	64.33	118.774	88.247	
3	154.67	90.141	92.486	92.486	43.509	72.73	121.864	
4	140.205	79.329	66.662	66.662	40.746	87.981	116.237	
5	128.59	62.333	62.478	62.478	53.358	36.842	69.843	
6	155.413	35.462	64.834	64.834	37.504	57.964	69.046	
7	54.668	71.458	45.012	45.012	82.987	92.196	78.319	
8	35.681	74.056	48.586	48.586	68.904	53.981	73.563	
9	45.963	63.93	133.805	133.805	70.1	133.097	58.719	
10	31.817	51.937	72.618	72.618	45.977	64.735	47.598	
11	228.338	88.227	80.598	80.598	79.247	47.137	64.152	
12	112.211	89.842	72.69	72.69	121.565	82.096	73.713	
13	117.665	78.395	83.383	83.383	93.311	91.852	56.392	
14	106.593	70.621	65.373	65.373	66.764	75.29	30.97	
15	57.74	69.663	120.959	120.959	71.29	125.887	50.532	
16	88.766	65.139	135.573	135.573	35.961	80.358	21.249	
17	52.736	68.702	84.824	84.824	38.066	58.362	167.668	
18	103.155	50.476	48.953	48.953	48.631	54.971	74.387	
19	93.672	56.754	72.153	72.153	50.392	60.461	108.776	
20	51.191	46.48	91.127	91.127	52.957	60.459	94.741	
21	83.824	70.083	127.491	127.491	39.349	66.175	80.263	
22	75.104	83.874	76.131	76.131	82.288	43.621	40.112	
23	134.535	58.388	56.298	56.298	57.348	87.358	79.085	
24	81.813	33.514	48.237	48.237	102.63	48.192	103.131	
25	98.335	111.54			67.063		67.679	
26	55.917	80.991			70.216		27.98	
27	65.992	110.177			55.463		123.844	
28	116.409	68.98			52.954		79.4	
29	164.912	71.525			55.964			
30	61.235	71.525			50.622			
31	77.201	119.092			29.845			
32	43.844	88.242			121.275			
33	96.141				64.802			
34	68.965				68.234			
35	96.957				64.449			

36	52.362				50.573			
37	84.103							
38	78.407							
39	83.217							
40	50.327							
41	67.104							
42	64.083							
43	87.258							
44	39.73							
45	73.877							
46	67.948							
47	44.491							
48	35.365							
49	96.628							
50	24.866							
51	69.216							
52	38.178							
53	78.364							
54	52.275							

Table 7*. Collection of pore diameter measurements for each image of 1.0% Alginate/1.0% Gelatin*

500x	1_001	1_002	1_003	1_005	1_007	1_008	
1	Length	Length	Length	Length	Length	Length	Average (um)
2	43.68	55.724	31.494	49.201	96.272	113.082	41.31450459
3	54.923	41.144	42.149	41.024	54.53	119.101	
4	43.76	43.829	17.782	29.374	113.334	59.474	
5	43.274	41.941	15.343	27.317	57.435	49.689	
6	54.512	37.169	41.691	23.765	80.629	64.768	
7	51.973	36.8	44.169	28.439	102.515	75.909	
8	40.914	45.093	28.51	33.635	74.249	90.471	
9	37.528	37.353	37.368	26.243	50.087	96.048	
10	31.426	54.458	40.331	33.531	45.515	102.992	
11	35.729	32.902	31.434	35.197	35.806	67.846	
12	50.456	35.864	25.251	30.434	92.231	76.888	
13	42.287	22.286	26.421	20.689	78.565	59.697	
14	41.999	53.258	40.255	23.111	86.204	86.486	
15	38.253	40.686	28.331	24.54	67.047	60.01	
16	40.284	38.517	23.405	49.296	87.994	75.026	
17	42.812	32.457	19.105	35.635	73.516	74.227	
18	46.778	36.658	39.556	19.172	54.597	94.747	

19	45.796	22.318	29.235	17.306	53.182	90.853
20	46.537	43.562	41.691	21.527	89.834	51.249
21	31.393	30.005	25.543	16.261	66.977	37.98
22	40.295	52.202	32.024	68.867	78.055	85.256
23	23.79	26.629	26.727	50.064	35.173	98.213
24	41.255	28.895	44.874	32.509	73.545	77.363
25	28.786	40.985	36.507	47.201	61.081	36.765
26	35.135	48.709	24.408	49.556	72.483	94.279
27	22.728	38.818	36.215	31.933	74.062	64.476
28	36.757	38.184	28.464	31.745	53.108	96.581
29	25.497	28.739	17.124	32.252	48.008	80.264
30	41.372	41.938	34.518	23.839	78.691	73.581
31	23.71	25.543	18.337	20.312	94.014	72.087
32	58.837	36.977	24.018	37.652	52.324	63.43
33	44.982	23.744	26.808	26.398	85.648	53.369
34	60.649	57.361	28.895	24.516	55.328	45.691
35	40.856	36.07	34.857	15.174	55.896	37.36
36	50.595	55.654	51.352	23.25	157.491	30.275
37	43.274	45.488	34.77	20.398	62.863	32.973
38	49.343	49.092	32.345	24.918	72.789	64.804
39	39.817	33.623	37.099	18.291	37.582	45.073
40	57.818	43.359	38.949	40.44	75.739	23.882
41	50.528	36.8	40.789	20.007	49.485	17.83
42	29.493	39.042	43.479	37.528	14.554	92.836
43	27.562	33.636	25.343	29.73	16.053	54.324
44	63.967	44.87	44.679	26.744		68.838
45	34.497	51.085	30.208	16.502		70.594
46	105.405	34.116	21.469	29.537		92.355
47	95.233	80.372	19.196	27.285		79.694
48	42.511	56.158	44.454	19.042		
49	25.382	24.265	32.818	11.467		
50	50.952	29.295	15.671	18.74		
51	37.547	13.574	14.232	12.984		
52	35.285	15.094	20.485	22.169		
53	27.905	28.053	18.305	17.846		
54	50.395	37.024	45.006	25.957		
55	34.476	35.779	33.414	18.67		
56	45.793	27.751	27.281	17.968		
57	36.757	20.207	24.851	18.95		
58	49.308	29.155	39.201	16.008		
59	41.308	36.183	37.647	16.887		
60	47.055	28.218	48.277	7.568		
61	34.662	20.3	41.868	8.915		
62	49.571	36.123	28.895	39.117		
63	32.522	33.475	33.428	35.896		
64	32.347	35.469	21.57	47.58		
65	33.531	50.415	24.018	39.755		

66	38.564	39.881	21.469	60.075			
67	25.946	51.131	21.997	29.73			
68	38.836	38.046	42.802	59.275			
69	35.4	39.368	41.593	47.03			
70	44.037	35.04	41.186	38.621			
71	33.435	33.636	30.174	32.933			
72	41.042	84.194	37.024	55.56			
73	29.109	67.463	32.902	23.808			
74	22.997	29.845	13.776	24.54			
75	23.937	28.592	12.293	26.393			
76	19.111	45.145	25.262	26.398			
77	14.635	40.403	22.744	11.867			
78	22.709	21.024	30.633	14.147			
79	27.183	23.486	26.305	13.018			
80	27.355	54.471	19.88	25.497			
81	24.004	51.673	18.775	22.728			
82	33.726	31.641	29.155				
83	30.735	33.618	36.914				
84	43.74	37.913	34.77				
85	49.4	27.829	35.616				
86		36.634	54.902				
87		45.135	26.465				
88		33.441	25.406				
89		27.493	15.717				
90		19.77	18.829				
91		26.672	16.253				
92			35.317				
93			35.633				
94			31.92				
95			17.022				